ISSN 1810-2328, Journal of Engineering Thermophysics, 2021, Vol. 30, No. 3, pp. 494–507. © Pleiades Publishing, Ltd., 2021.

A Numerical Investigation of Heat Transfer from Heated Surfaces of Different Shapes

D. E. Alnak[1*], F. Koca[1], and Y. Alnak[1***]**

[1] *Sivas Cumhuriyet University, Technology Faculty, Automotive Engineering Department, Sivas, Turkey*

Received April 6, 2021; in final form, July 18, 2021; accepted July 26, 2021

Abstract—The object of this study was cooling of inverted and plain triangular profile copper surfaces at a constant heat flux of 1000 W/m^2. The cooling of these triangular profile surfaces placed at the bottom of a rectangular channel was carried out using a single jet of air flow. The 3D geometry was analyzed with the steady state and k-ε turbulence models using the Ansys-Fluent software program. While all surfaces of the rectangular channel were adiabatic, a constant heat flux was applied to the triangular profile surfaces. The impingement air jet had an inlet temperature of 300 K. The Re number range in the study was 4000–10000, the interval between the jet and plate H/D_h being equal to 4, 6, 10, and 12. The results obtained were compared with experimental and numerical results in literature, which showed their compatibility. The results are presented as the average Nu number and the surface temperature variations for the profiled surfaces of both inverted and plain triangular profiles. The velocity, streamline, and temperature contour distributions of the jet flow along the channel were analyzed for both profiles for different H/D_h ratios. The average Nu number value was found to be 49.67% higher for the inverted triangular profile surfaces than that for the plain profile surfaces for Re of 4000 to 10000 and $H/D_h = 10$.

DOI: 10.1134/S1810232821030127

1. INTRODUCTION

Flow regulation through jet impact heat transfer is widely used in the industry [1]. Impinging jets are widely used in various engineering and industrial fields as an effective heat/mass transfer tool, including applications like cooling of various gas turbine blades and electronic devices, food processing, drying of fabric and paper materials, tempering of metals, and many other applications [2, 3]. Since the technology development in recent years has made electronic elements with high heat generation smaller in size, adequate cooling performance cannot be achieved using only air cooling. Use of impinging jet for cooling purposes enables removal of great amounts of heat from devices with high heat flux [4, 5].

There are lots of studies on the heat transfer with impinging jets. The first studies on the jet flow date back to 1951 [6]. That study was followed by the analytical and experimental work on multiple jet arrays by Kezios in 1956 [7]. The average heat transfer coefficients generated by impingement jets outflowing from circular cells were measured. Since that time, many researchers have tried both numerical and experimental approaches. Argus et al. [8] investigated numerically the characteristics of fluid flow and heat transfer in cooling of heated block arrays in a channel by a single slot air jet. They performed experiments for different Re number values, channel heights, slot jet hole widths, distances to impinged plates, block heights, and thermal conductivity coefficients. They stated the cooling of the blocks to be efficient with increasing Re number and decreasing channel height.

Lee et al. also performed numerical studies using the finite volume method [9]. The effect of the Re number in the range of 50–500 and channel height ratios varying from 2 to 5 was investigated for a 2D unsteady flow. They reported the pressure coefficient, skin friction coefficient, and Nu number

[*] E-mail: dealnak@cumhuriyet.edu.tr
[**] E-mail: ferhatkoca@cumhuriyet.edu.tr
[***] E-mail: ytas@cumhuriyet.edu.tr

to differ from those in a steady flow. Yang et al. [10] investigated the flow and heat characteristics using a turbulent slot jet impinging on a semi-circular concave surface. They used the k-ε model solution obtained by the finite difference method to solve the governing equations with variations of the Re number ($5920 < \mathrm{Re} < 23700$), dimensionless jet slot-to-plate surface distance H/B ($0.5 < \mathrm{H/B} < 12$), dimensionless jet slot width B/D ($0.033 < \mathrm{B/D} < 0.05$), and heat flux q ($1663\ \mathrm{W/m^2} < q < 5663\ \mathrm{W/m^2}$). The maximum Nu value was at the stagnation point. Huang et al. [11] investigated the fluid flow and heat transfer characteristics with the effect of cavity and impinging jet. They showed that a surface with a convex cavity was more efficient in terms of cooling as compared with surfaces without cavities, with mixed cavities, and with concave cavities. They also indicated that convex cavities could reduce the flow resistance in a microchannel sink with a jet flow.

Olsson et al. [12] used a multi-slot impinging jet flow on a cylinder surface for heat transfer and flow predictions with application of computational fluid dynamics. They obtained results at the Re number varying from 23,000 to 100,000 and different arrangements of impinging jets. They found the flow characteristics and heat transfer to depend on the jet arrangement. They also report higher heat transfer with increase in the Re number. Mushatat [13] numerically analyzed impingement jets with different parameters to determine the heat transfer and turbulent air flow properties. The size, number, and arrangement of jets and ribs were selected variable. According to the results of the study, the local Nu number and the size of the recirculation zones grew with the ratio of the slot jet width to the rib thickness B/W and decreased with the ratio of the channel height to the slot jet width H/B. The investigation also showed that the distance between the jets and the Re number value significantly affected the local Nu number, recirculation region, and turbulence kinetic energy.

Alnak et al. [14] numerically investigated cooling of heated triangular profile surfaces with a fluid of constant temperature provided by an air jet. They analyzed the system for a turbulent flow at certain boundary conditions. The basic parameters in their study were the distance between the jet and the impacted surface and the Re number. When the Re number was built up from 4000 to 6000, they achieved an increase of 69.32% in the average Nu number at a dimensionless jet-plate distance of 6. They detected the highest surface temperature on the last heated surface since the jet effect of the fluid decreased towards the outlet of the channel. In general, they emphasized that the Re number and the jet-plate distance had significant influence on the Nu number. Karabulut [15] investigated numerically the heat and flow properties of five different reverse and straight circle profile surfaces placed in rectangular channels. He used a computational fluid dynamic solution for 3D steady and turbulence models. The investigation parameters were the Re number range from 4000 to 10,000 and the jet-plate distance ratios varying from 4 to 12. According to his results, the jet-plate distance ratio and the Re number had serious influence on the heat transfer and thus they can be used for cooling of surfaces.

Fahroz et al. [16] used ANSYS Fluent to study numerically the heat transfer from an isothermally heated flat surface under turbulent twin oblique confined slot-jet impingement. The parametric study was conducted through variation of the jet exit Re number ($\mathrm{Re} = 23{,}000$ and 50,000), distance between two jets ($\mathrm{L} = 0$, 2, and 4), distance between the jet exit and the heated plate ($\mathrm{H} = 2.6$, 4, and 6), and the angle of jet inclination to the impingement surface ($45° < \theta < 90°$). The results show that when the angle of the jet was reduced from 90° (normal jet), the Nu number on the impingement surface decreased gradually. The influence of change in the Re number and jet angle Nu number exceeded the effect of variation of combination of the L and H values.

Leena et al. [17] investigated numerically and experimentally the heat transfer characteristics of multiple air jet flow impinging on a stationary flat copper plate. They used the finite volume method in the Ansys-Fluent software program for the numerical study and designed and fabricated a system for the experimental part at the bottom surface of a copper plate heated for the simulation. The Re number (4000–8000) and the distance between the jets were the parameters. The cooling was optimum in the case of a Re number of 5000.

In the work, following studies in literature, 50×200 mm rectangular channels were used, as well an impinging jet flow of air at a temperature of 300 K. The variable parameters were the geometrical shapes of the surfaces profiled as inverted and plain triangles, the distance between the bottom surface of the channel and the jet $\mathrm{H/D_h}$, and Re number value. In all the different geometric cases, a constant heat flux of $1000\ \mathrm{W/m^2}$ was applied to the triangular profile surfaces. The scope of the Re number on the impinging jet was 4000–10,000 and the distance between the impinging jet and the bottom plate surface was in the range of 4–12 $\mathrm{D_h}$. The turbulence-governing equations were solved by the finite

volume method with the well-known 3D steady-state k-ε turbulence model using the Ansys-Fluent software. The numerical results of the present study were compared with numerical and experimental results in literature, and the results were found to be compatible. The results were presented as the average Nu number and surface temperature changes for all the inverted and plain triangular profile surfaces and analyzed via comparison with each other. The streamline, temperature, and velocity contour distributions of the impinging jet flow along the channel for different H/D_h ratios and different Re numbers have been evaluated for the inverted and plain triangular profile surfaces.

2. NUMERICAL METHOD

In this study, the forced convection heat transfer of jet flow on surfaces with different geometric profiles was solved numerically as steady and three dimensional using the Ansys-Fluent analysis software.

For the governing equations, the convergence scale was 10^{-6} for the energy equation and 10^{-7} for the momentum equation. The tetrahedral structure was used for the mesh in the simulations. However, the well-known standard k-ε turbulence model was employed in the numerical solutions for triangular profile surfaces.

The solutions of the heat transfer and flow characteristics along the channel with different triangular profile surfaces were obtained from solutions of partial differential equations. These equations were derived from the time-averaged mass, momentum, and energy conservation equations for a turbulent flow under steady-state and incompressible conditions without body forces as described below [18].

The continuity equation:

$$\frac{\partial \bar{u}}{\partial x}+\frac{\partial \bar{v}}{\partial y}+\frac{\partial \bar{w}}{\partial z}=0. \tag{1}$$

The momentum equations:

the x direction momentum equation,

$$\left[\bar{u}\frac{\partial \bar{u}}{\partial x}+\frac{\partial \overline{(u')^2}}{\partial x}\right]+\left[\bar{v}\frac{\partial \bar{u}}{\partial y}+\frac{\partial \overline{(u'v')}}{\partial y}\right]+\left[\bar{w}\frac{\partial \bar{u}}{\partial z}+\frac{\partial \overline{(u'w')}}{\partial z}\right]=-\frac{1}{\rho}\frac{\partial \bar{p}}{\partial x}+v\left(\frac{\partial^2 \bar{u}}{\partial x^2}+\frac{\partial^2 \bar{u}}{\partial y^2}+\frac{\partial^2 \bar{u}}{\partial z^2}\right), \tag{2.1}$$

the y direction momentum equation,

$$\left[\bar{u}\frac{\partial \bar{v}}{\partial x}+\frac{\partial \overline{(v')^2}}{\partial x}\right]+\left[\bar{v}\frac{\partial \bar{v}}{\partial y}+\frac{\partial \overline{(v'v')}}{\partial y}\right]+\left[\bar{w}\frac{\partial \bar{v}}{\partial z}+\frac{\partial \overline{(v'w')}}{\partial z}\right]=-\frac{1}{\rho}\frac{\partial \bar{p}}{\partial y}+v\left(\frac{\partial^2 \bar{v}}{\partial x^2}+\frac{\partial^2 \bar{v}}{\partial y^2}+\frac{\partial^2 \bar{v}}{\partial z^2}\right), \tag{2.2}$$

the z direction momentum equation,

$$\left[\bar{u}\frac{\partial \bar{w}}{\partial x}+\frac{\partial \overline{(w')^2}}{\partial x}\right]+\left[\bar{v}\frac{\partial \bar{w}}{\partial y}+\frac{\partial \overline{(w'v')}}{\partial y}\right]+\left[\bar{w}\frac{\partial \bar{w}}{\partial z}+\frac{\partial \overline{(w'w')}}{\partial z}\right]=-\frac{1}{\rho}\frac{\partial \bar{p}}{\partial z}+v\left(\frac{\partial^2 \bar{w}}{\partial x^2}+\frac{\partial^2 \bar{w}}{\partial y^2}+\frac{\partial^2 \bar{w}}{\partial z^2}\right). \tag{2.3}$$

The energy equation:

$$\left[\bar{u}\frac{\partial \bar{T}}{\partial x}+\bar{v}\frac{\partial \bar{T}}{\partial y}+\bar{w}\frac{\partial \bar{T}}{\partial z}\right]+\left[\frac{\partial \overline{(u'T')}}{\partial x}+\frac{\partial \overline{(v'T')}}{\partial y}+\frac{\partial \overline{(w'T')}}{\partial z}\right]=\frac{k}{\rho c_p}+v\left(\frac{\partial^2 \bar{T}}{\partial x^2}+\frac{\partial^2 \bar{T}}{\partial y^2}+\frac{\partial^2 \bar{T}}{\partial z^2}\right)+\varphi. \tag{3}$$

The steady flow turbulence kinetic energy equation:

$$\left[\frac{\partial(\rho u k')}{\partial x}+\frac{\partial(\rho v k')}{\partial y}+\frac{\partial(\rho w k')}{\partial z}\right]=\frac{\partial}{\partial x}\left(\frac{\mu_t}{\sigma_k}\frac{\partial k'}{\partial x}\right)+\frac{\partial}{\partial y}\left(\frac{\mu_t}{\sigma_k}\frac{\partial k'}{\partial y}\right)+\frac{\partial}{\partial z}\left(\frac{\mu_t}{\sigma_k}\frac{\partial k'}{\partial z}\right)+\mu_t\varphi-\rho\varepsilon. \tag{4}$$

The turbulence viscosity:

$$\mu_t = C'_\mu \rho \frac{k'^2}{\varepsilon}. \tag{5}$$

In the k-ε turbulence model used in the present study, ε indicates the turbulence distribution, while k' and ϕ stay for the turbulence kinetic energy and viscous dissipation term, respectively.

The turbulence kinetic energy:

$$k' = \frac{1}{2}\left(\overline{u'^2} + \overline{v'^2} + \overline{w'^2}\right). \tag{6}$$

The viscous dissipation term:

$$\varphi = 2\mu\left[\left(\frac{\partial u}{\partial x}\right)^2 + \left(\frac{\partial v}{\partial y}\right)^2\right] + \mu\left(\frac{\partial u}{\partial x} + \frac{\partial u}{\partial y}\right)^2. \tag{7}$$

The turbulence kinetic energy disappearance equation:

$$\frac{\partial(pu\varepsilon)}{\partial x} + \frac{\partial(pv\varepsilon)}{\partial y} + \frac{\partial(pw\varepsilon)}{\partial z} = \frac{\partial}{\partial x}\left(\frac{\mu_t}{\sigma_\varepsilon}\frac{\partial \varepsilon}{\partial x}\right) + \frac{\partial}{\partial y}\left(\frac{\mu_t}{\sigma_\varepsilon}\frac{\partial \varepsilon}{\partial y}\right) + \frac{\partial}{\partial z}\left(\frac{\mu_t}{\sigma_\varepsilon}\frac{\partial \varepsilon}{\partial z}\right) + C_{1\varepsilon}\mu_t\frac{\varepsilon}{k'}\varphi - C_{2\varepsilon}\rho\frac{\varepsilon^2}{k'}. \tag{8}$$

The model constants C_μ, $C_{1\varepsilon}$, $C_{2\varepsilon}$, σ_k, and σ_ε are typical default values used in the standard k-ε turbulence model [18]. The values of these constants resulted from numerous data fitting iterations for many turbulent flows.

The calculation of the Re number was done with the equation

$$\mathrm{Re} = \frac{V_\infty \mathrm{D_h}}{v}. \tag{9}$$

D_h is referred to as the hydraulic diameter of the jet inlet and is calculated as follows:

$$\mathrm{D_h} = \frac{4A_c}{P} = \frac{4(aW)}{2(a+W)}. \tag{10}$$

In this hydraulic diameter equation, A_c is the cross-sectional area and P is the perimeter length of the jet inlet.

The Nu number is considered to be the ratio between the convection heat transfer rate and the conduction heat transfer rate. The local Nu number is calculated from the following equation.

$$-k\left(\frac{\partial T}{\partial n}\right)_s = \mathrm{h}(T_\infty - T_S) \text{ and } \mathrm{Nu} = \frac{\mathrm{hD_h}}{k}. \tag{11}$$

Here, h is the local heat transfer coefficient on the surface and n is the direction perpendicular to the surface.

Calculation of the mean heat transfer coefficient:

$$h_m = \frac{1}{L}\int_0^L h dx. \tag{12}$$

Calculation of the mean Nu number:

$$\mathrm{Nu}_m = \frac{h_m \mathrm{D_h}}{k}. \tag{13}$$

3. GEOMETRIC MODEL

Figure 1 shows the channels with triangular profile surfaces used in the study with the boundary conditions and dimensions. The hydraulic diameter D_h of the jet nozzle was 9.9 mm; the flow channel length L was 200 mm; the channel width W was 50 mm. The jet nozzle was a 5.5 × 50 mm rectangle and provided a flow with a uniform velocity profile. The inlet velocity range of the fluid supplied from the jet nozzle to the channel was 6.23–15.58 m/s. The channel height was also chosen as a variable parameter depending on the hydraulic diameter: $4 \times D_h$, $6 \times D_h$, $10 \times D_h$, and $12 \times D_h$. There were five inverted and five plain triangular profile surfaces in two different channels. In addition, the distance between two profile elements being D_h, the profile width and height were $2 \times D_h$ and D_h, respectively, depending on the jet nozzle hydraulic diameter.

The following assumptions were made in this study.

a) The flow field for the channels was three-dimensional, steady, and turbulent.

b) The jet fluid used to cool the triangular profile surfaces was incompressible air.

c) The constant heat flux on the triangular profile surfaces was 1000 W/m^2.

d) The thermal properties of the jet fluid were constant.

e) There was no heat generation for the triangular profile surfaces and the jet fluid.

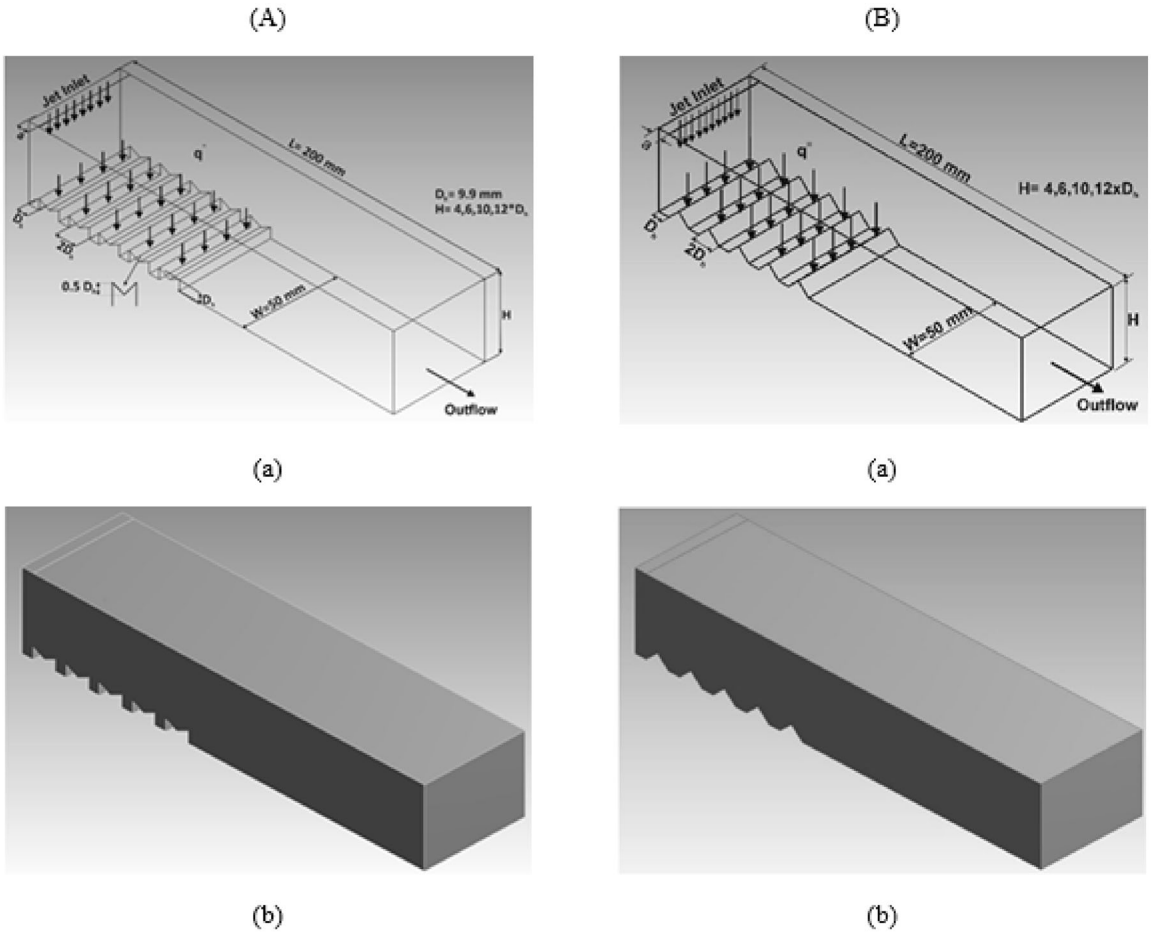

Fig. 1. Channel perspective view with (A) inverted triangular and (B) plain triangle profiles; (a) calculation medium with boundary conditions and dimensions; (b) CFD simulation medium.

4. RESULTS AND ASSESSMENT

Compatibility of the accuracy of numerical studies with literature is very important. Therefore, Fig. 2 shows the Nu number results of the experimental and numerical studies by Kılıç et al. [19] for H/D = 6 and Re = 6000 and 8000 in comparison with the numerical results of the present study. The 200 × 50 mm plain copper plate surface used by Kılıç et al. was utilized in this study. When the Nu number value in the impingement jet flow area at Re = 6000 was examined, it was found that the deviation between the experimental result by Kılıç et al. and the numerical result of this study was 3.99%. When the numerical results of the two studies were compared, this difference was found to be 1%. However, at Re = 8000, the deviation between the experimental result by Kılıç et al. and the numerical result of this study was

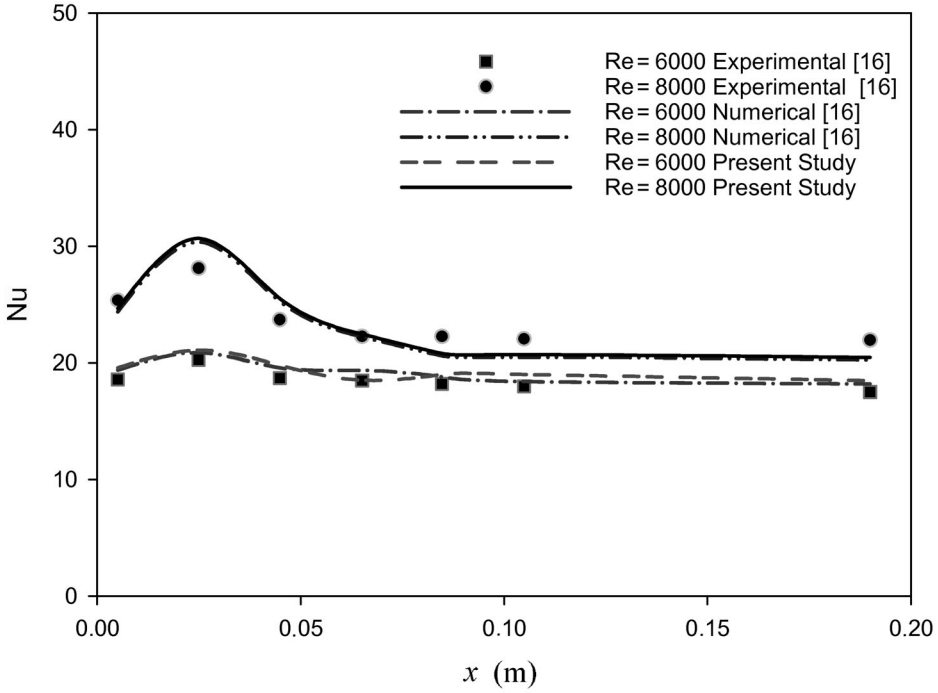

Fig. 2. Comparison of experimental and numerical results by Kılıç et al. [19] with results of presented numerical study.

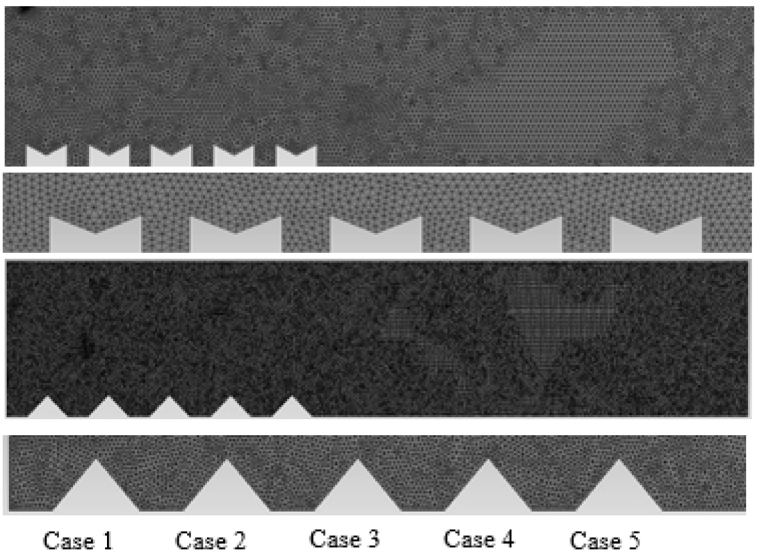

Fig. 3. Mesh structures used in calculations inverted and plain triangular patterned surfaces.

Mesh independence results for Nu_m and T_{mojet} for channels with inverted triangular profile (A) and plain triangular profile (B) surfaces

A		
Mesh number	Nu_m	$T_{out-jet}$ (K)
1,875,046	8.3159	328.56
3,476,017	8.3158	328.73
4,578,246	8.3158	328.73
B		
Mesh number	Nu_m	$T_{out-jet}$ (K)
1,458,421	10.8701	321.829
1,658,422	10.8719	321.838
1,845,145	10.8718	321.837

9.15% due to the increase in the turbulence density in the impingement region. The deviation between the numerical results was 1.02% in the same region. From these data and graphs, it can be inferred that the numerical results of the present study can be compared with the numerical and experimental results by Kılıç et al. [19] and thus the numerical present study is reasonable and appropriate.

For determination of the influence of the mesh number on the mean Nu number of triangular profile surfaces and the outlet temperature of the jet flow from the channel for $H/D_h = 4$ and Re = 4000, the table presents the mesh independence analysis results for the inverted and plain triangular profile surfaces, see A and B, respectively. From the results, it was determined that 3,476,017 and 1,658,422 mesh elements, respectively, were sufficient for the channels with the inverted triangular profile surfaces. The mesh structures of the channels with the inverted and plain triangular profile surfaces are also shown with A and B in Fig. 3. At the same time, zoomed images are given for better presentation of the mesh structures of the triangular profile surfaces.

Figure 4 presents the influence of the Re numbers (4000, 6000, 8000, and 10,000) and the channel heights ($H/D_h = 4$, 6, 10, and 12) on the average Nu numbers of the profiled surfaces for different cases (Patterns 1, 2, 3, 4, and 5) of the inverted and plain triangular profile surfaces. The pattern numbers in the graphs indicate the order of placement of the surfaces starting from the left side of the channel. As the jet velocity increased, which enhanced the turbulence density, the Nu number on the surfaces of the profiles also grew. For both profiles, there were recirculation zones to the left at the bottom of the channel wall for all Re numbers. Due to this recirculation, the highest Nu number value for Pattern 2 was reached for the inverted triangular profile surfaces due to the change in the direction of the jet flow on the surfaces. However, since this recirculation effect for the plain triangular profile surfaces is limited, the obtained Nu number values are higher for Pattern 1 at all values of H/D_h. In addition, Pattern 1 in the channel was the surface with the highest temperature difference between the jet fluid and the pattern surface, which implies the highest heat transfer. However, while the Nu number grew for $H/D_h = 4$ to 10 because of the recirculation zones formed within the channel for the plain triangle profile surfaces and decreased for $H/D_h = 12$, the Nu number diminished with increasing H/D_h for the inverted triangle profile surfaces. Pattern 5, which has the least Nu number values because the recirculation directed the jet fluid movement, was the last row surface in the channel. However, for the inverted triangular profile surface, the average Nu number increase was 49.67% for Re varying from 4000 to 10,000 and $H/D_h = 10$, while this increase value was 48% for the plain triangular profile surface. Besides, the Nu number was less sensitive to the H/D_h increase as compared with the increase in the Re number.

Figure 5 presents the mean surface temperatures of the inverted and plain triangular profiles for jet-to-plate distances H/D_h of 4, 6, 10, and 12 and the Re numbers. Growth of the Reynolds number increases the turbulence density of jet flow inside the channel and thus the heat transfer from the profiled surfaces, which ensures decrease in the surface temperatures at all channel heights investigated.

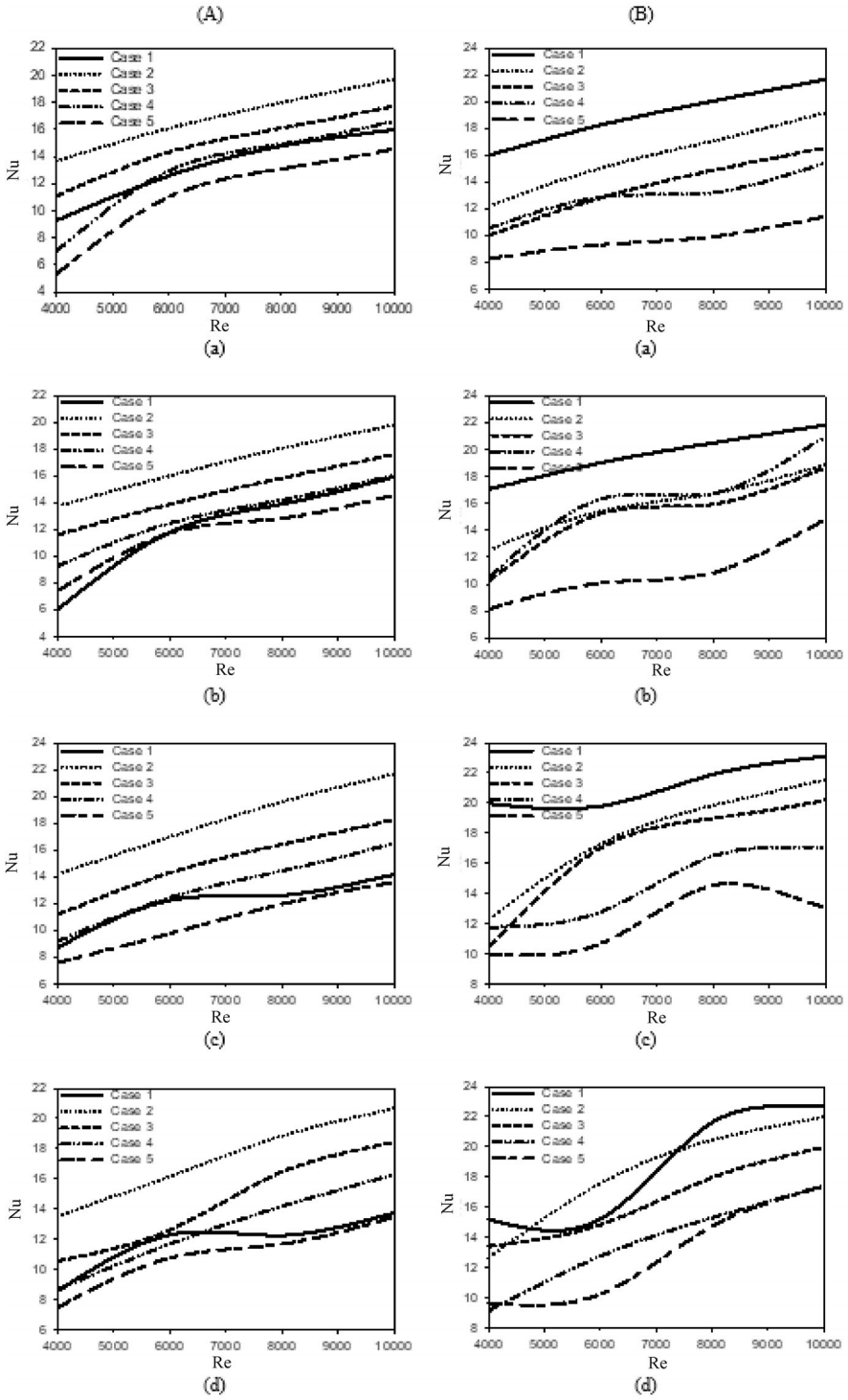

Fig. 4. Mean Nu number versus Re number for H/D_h equal to (a) 4, (b) 6, (c) 10, and (d) 12 and inverted triangle (A) and plain triangle profile (B) surfaces.

From the graphs it is seen that the highest surface temperature was on the profiled surfaces at the exit of the channel (Pattern 5) for both profiles. However, because the recirculation directed the jet flows through the entrance of the channel, the surfaces for Patterns 2 (case 2) and 1 (case 1) had the lowest temperatures for inverted and plain profiles, respectively. Besides, the surface temperature values obtained for the plain triangle profiles were lower than those for the inverted triangular profiles. While

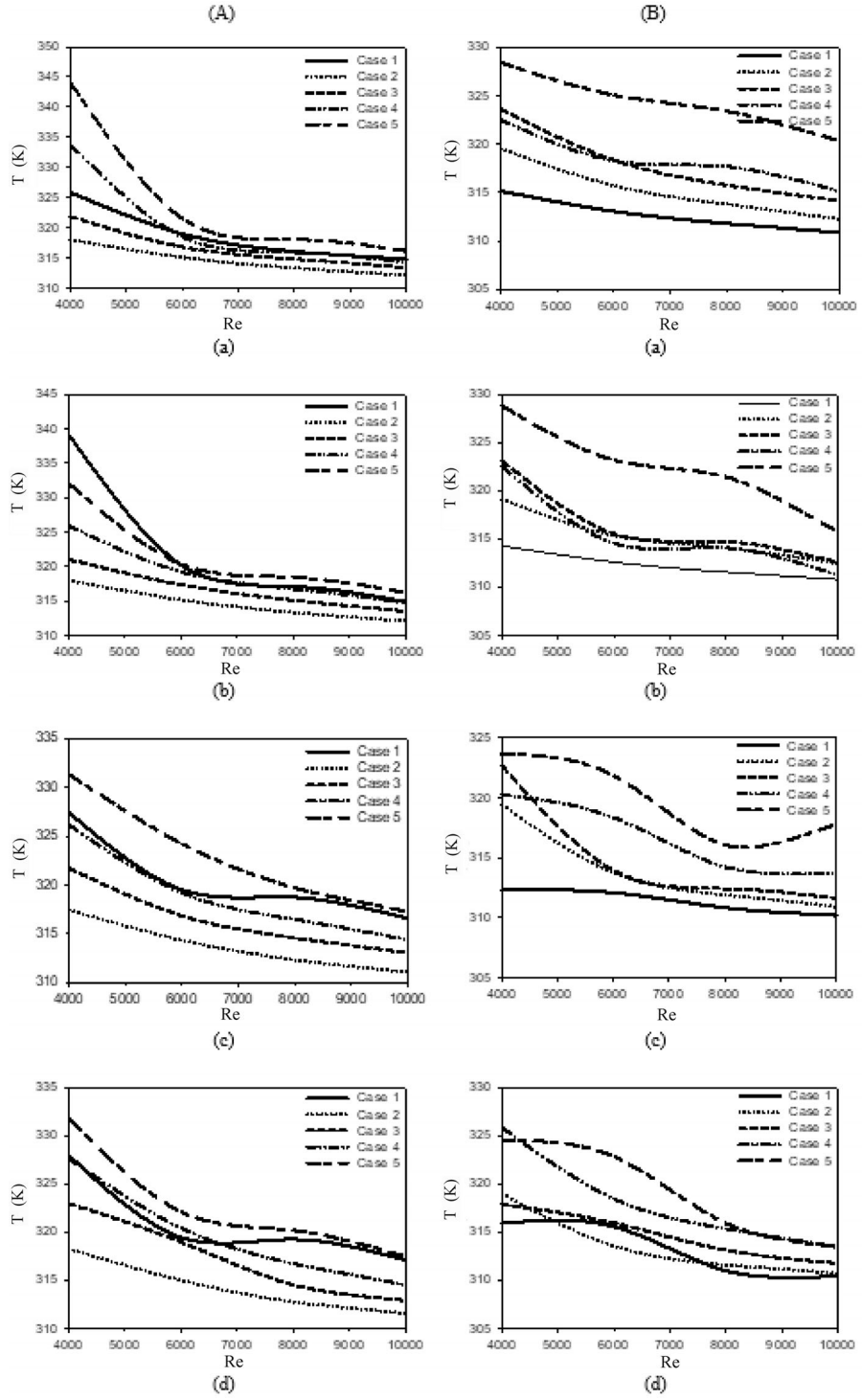

Fig. 5. Mean surface temperature versus Re number for H/D_h equal to (a) 4, (b) 6, (c) 10, and (d) 12 and inverted triangular (A) and plain triangular profile (B) surfaces.

the average surface temperature value for the inverted triangle profile was 324.812 K at $H/D_h = 10$ and Re = 4000, that of the plain triangle profile was 319.685 K at the same conditions.

Contour images are the most appropriate data for visual evaluation of the results, and therefore contour images of flow are presented in almost all numerical studies in the literature, the velocity, streamline, and temperature contours being of the highest interest. In this way it is easy to understand how a parametric variable causes changes in the system. Contour images are given in this section

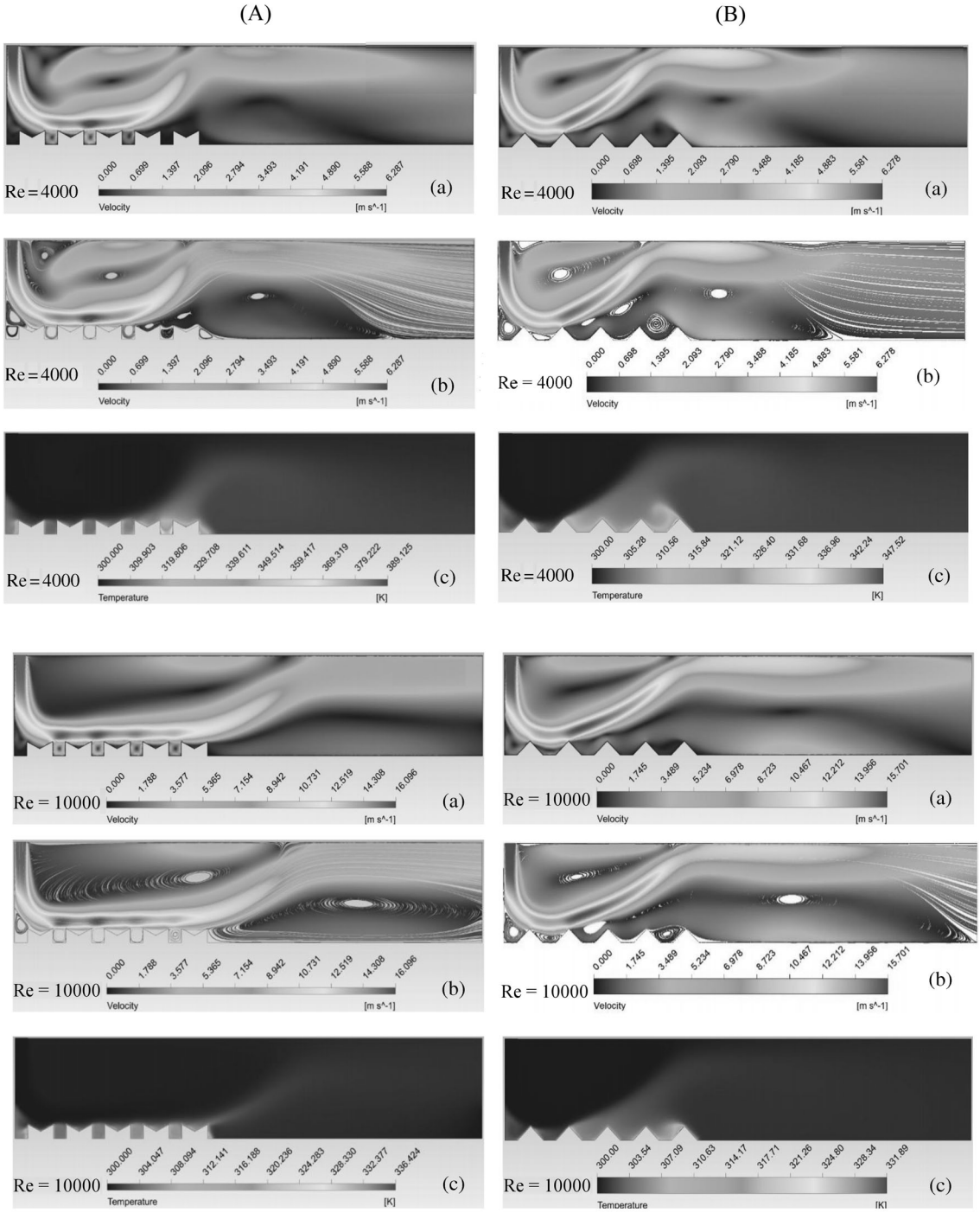

Fig. 6. Variations of (a) velocity, (b) streamline, and (c) temperature contour distribution with Re number for (A) inverted triangular and (B) plain triangular profile surfaces ($H/D_h = 4$).

for interpretation of the changes in the Re number and channel height/hydraulic diameter ratio as parameters determined in the study.

Figure 6 gives the velocity, streamline, and temperature contour distributions of inverted (A) and plain (B) triangular profile surfaces for $H/D_h = 4$ and Re = 4000 and 10,000. Recirculation happens to the left at the bottom of wall for surfaces of both profiles at the analyzed Re numbers. However, this recirculation directs the jet flow to the second pattern for the inverted triangular profile. Besides, the recirculation zones consist of areas where the jet flow separates from the surfaces and areas where the

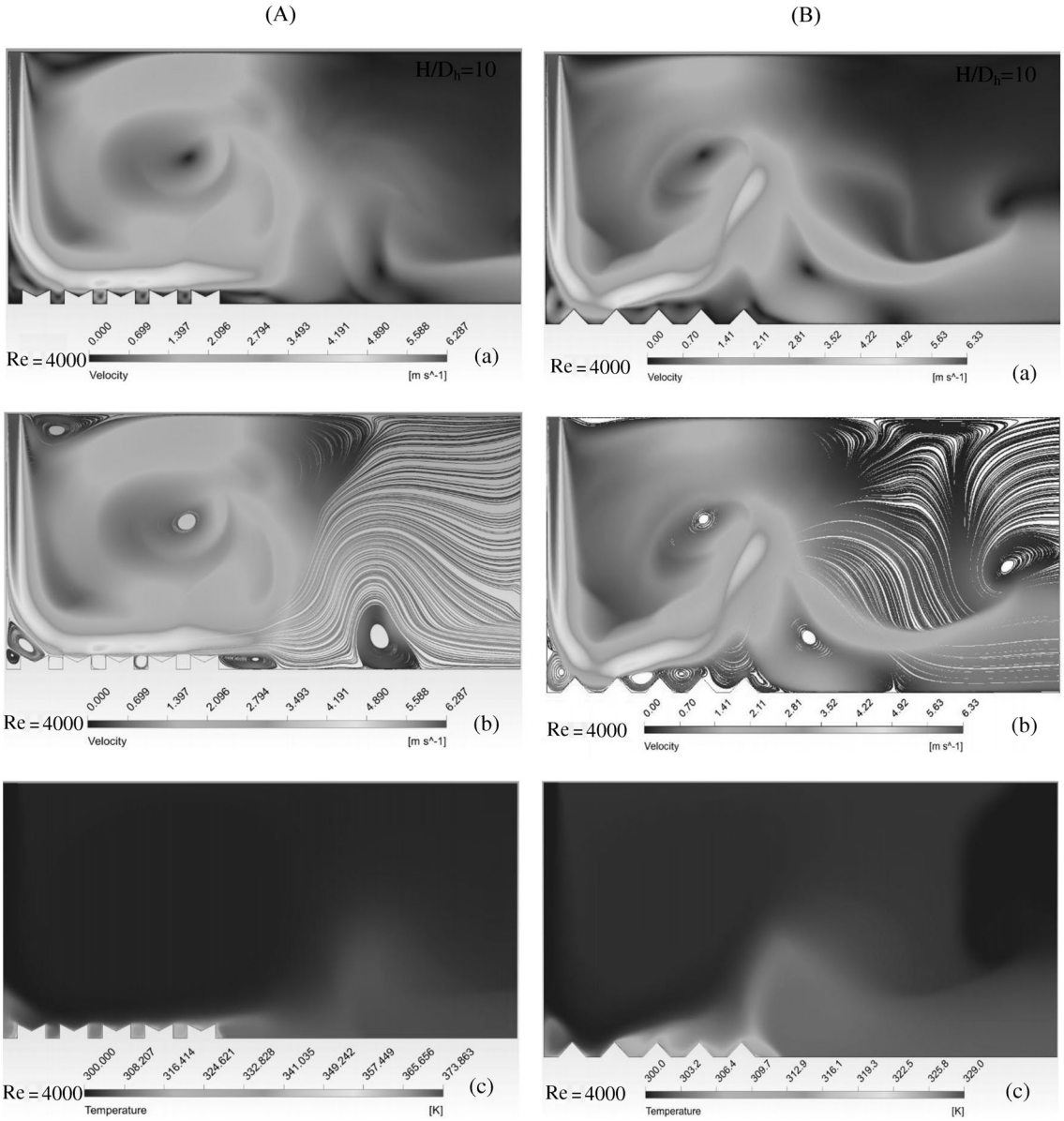

Fig. 7a. Variations of (a) velocity, (b) streamline, and (c) temperature contour distribution with Re number for (A) inverted triangular and (B) plain triangular profile surfaces ($H/D_h = 10$).

jet flow cannot get in between the patterns. In these parts, temperature increments occur, as can be seen from the temperature distribution contours. When the Re number grows from 4000 to 10,000, the recirculation zones combine and direct the jet flow to the profiled surfaces. So, because the jet effect was higher on the profiled surfaces, the heat transfer increased, and the profiled surfaces cooled down better.

Figure 7 presents the velocity, streamline, and temperature contour distributions for the inverted and plain triangular profile surfaces for $H/D_h = 10$ and Re numbers of 4000 and 10,000. While the H/D_h increased, the effect of the jet on the surfaces decreased. This case is seen in the velocity distribution contours with reduction of the velocity values on the profiled surfaces. However, the H/D_h increment reduces the turbulence density in the channel and enlarges the recirculation regions. Thus, while the temperature grows on the profiled surfaces, the recirculation regions combine, increasing the Re number, and direct the flow onto the profiles. Besides, at $H/D_h = 10$, the decrease in the surface temperature for Re = 10,000 as compared with Re = 4000 can be easily seen from the temperature contour distributions.

Examination of all the situations in Figs. 6, 7a, and 7b reveals the comparative effectiveness of the

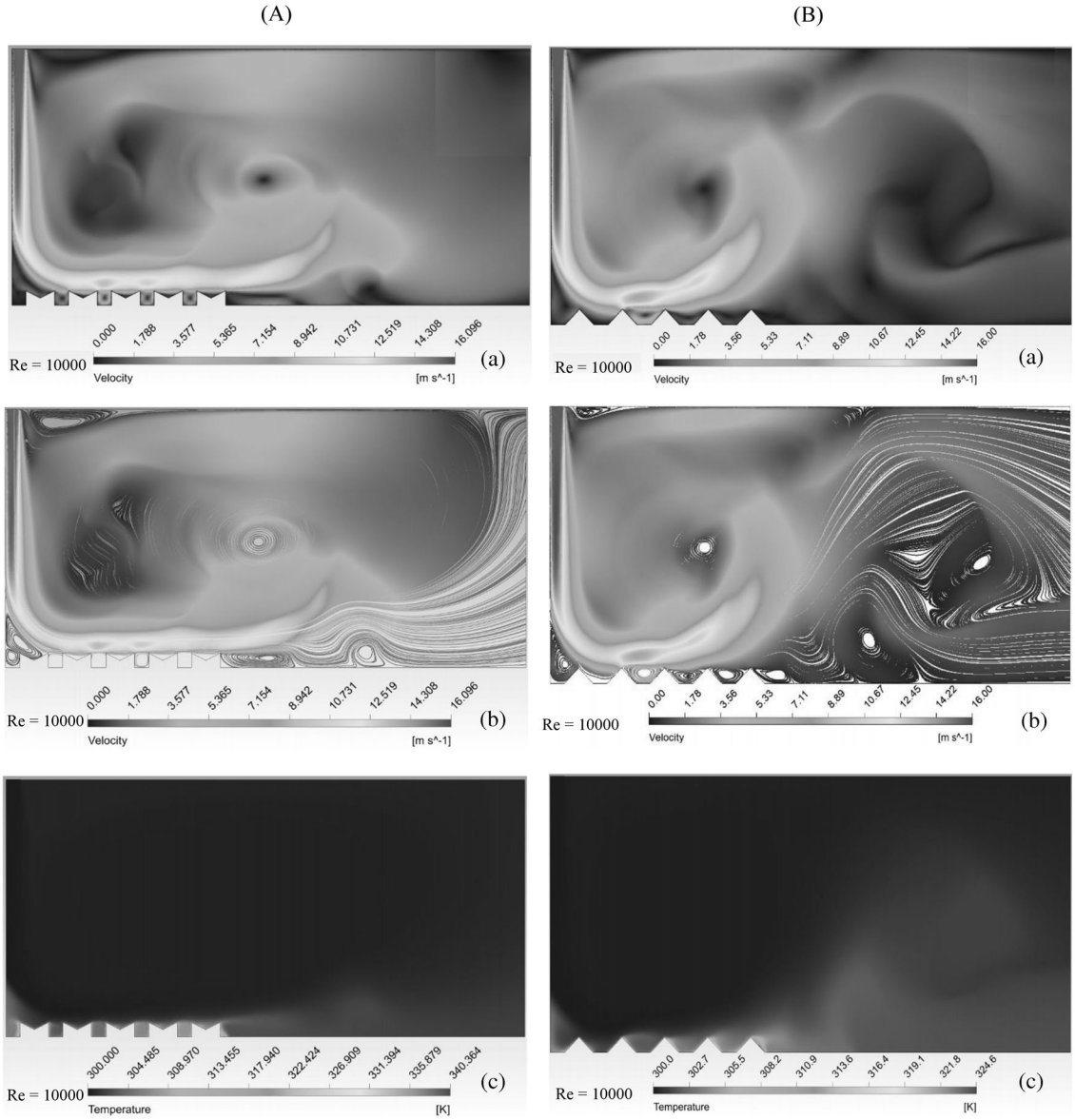

Fig. 7b. Variations of (a) velocity, (b) streamline, and (c) temperature contour distribution with Re number for (A) inverted triangular and (B) plain triangular profile surfaces ($H/D_h = 10$).

heat transfer as a result of the flow movement on the profiled surfaces and in the channel. One of the most important implications at this point is when the Re number increased from 4000 to 10,000 and the recirculation zones converged and directed the jet stream to the profiled surfaces. Thus, as the jet effect increased on the profiled surfaces, the heat transfer grew, and the profiled surfaces were cooled better.

5. CONCLUSION

The increment in the amount of heat produced per unit volume with the ongoing size reduction in the electronic element technology requires an effective cooling method. Impinging jets as an effective heat/mass transfer tool in applications like cooling of gas turbine blades and electronic devices, food processing, fabric and paper drying, annealing of metals, etc. are widely used in various industrial processes.

In this study, we analyzed numerically the heat transfer and flow structures in a rectangular channel of copper plate surfaces with inverted and plain triangular profiles under a constant heat flux using a

single air jet impinging flow. The results of this numerical study were compared with experimental and numerical results in the literature. The results were found to be compatible. The results were presented as the average Nu number and surface temperature variation for both inverted and plain triangular profile surfaces. The velocity, streamline, and temperature contour distributions of the air jet impingement flow within block channels were evaluated at variation of H/D_h and the Re number. All data obtained from the numerical study were summarized as follows.

—In general, the Nusselt number, which is the most important dimensionless value, grew with the Re number for both inverted and plain triangular profile surfaces. However, it can also be seen from the graphs that the Nu number values fluctuated depending on the recirculation regions that arose between the patterns.

—While the highest average Nu number values were reached on the second triangular profile surfaces due to the jet flow direction because of the recirculation region formed on the lower left sides of the channels for the inverted profile, the same occurred in the first pattern surfaces for the plain profile.

—For the inverted triangular profile surfaces, the average Nu number increase was 49.67% for Re = 4000 to Re = 10,000 for $H/D_h = 10$, while this increase was 48% for the plain triangular profile surfaces. Besides, the Nu number was less sensitive to the H/D_h increase as compared with the increase in the Re number.

—The surface temperature values obtained for the plain triangle profile were lower than those obtained for the inverted triangle profile. While the average temperature value of the inverted triangle profile surface was 324.812 K for $H/D_h = 10$ and Re = 4000, it was 319.685 K for the plain triangle profile at the same conditions.

—When the Re number grew from 4000 to 10,000, the recirculation zones combined and directed the jet flow to the profiled surfaces. So, because the jet effect was enhanced on the profiled surfaces, the heat transfer increased, and the profiled surfaces were cooled better.

—Besides, at $H/D_h = 10$, the decrease in the surface temperature for Re = 10,000 as compared with the surface temperature for Re = 4000 can be easily seen from the temperature contour distributions.

—In conclusion, the heat transfer, including the average Nusselt numbers, was significantly affected by the Reynolds numbers of the jet, while it was less sensitive to the jet-to-plate distance. It can also be concluded that the geometry of air flow jet and channel used in this study can be employed to cool electronic components because it is resembles various electronic equipment applications.

NOTATIONS

a—channel length of jet entry, mm
A_c—cross-section of jet, m^2
H—rectangular channel height, mm
L—rectangular channel length, mm
W—rectangular channel width, mm
D_h—hydraulic diameter of rectangular channel, m
h—convective heat transfer coefficient, $W \cdot m^{-2} \cdot K^{-1}$
k—heat conduction coefficient, $W \cdot m^{-1} \cdot K^{-1}$
V—inlet fluid flow velocity, $m \cdot s^{-1}$
c_p—specific heat of the fluid, $J \cdot kg^{-1} \cdot K^{-1}$
P—perimeter length of jet, m
p—pressure, $N \cdot m^{-2}$
q''—heat flux in profiled surfaces, $W \cdot m^{-2}$
T—temperature, K
u, v, w—velocity components of x, y, z directions, $m \cdot s^{-1}$
u', v', w'—fluctuating velocity components in x, y, z directions, $m \cdot s^{-1}$
$\bar{u}$, $\bar{v}$, $\bar{w}$—mean velocities in coordinates, $m \cdot s^{-1}$
Re—Reynolds number ($= V_\infty D_h/\nu$)
Nu—Nusselt number ($= hD_h/k$)

Greek Symbols

ρ—density, kg·m^{-3}
μ—dynamic viscosity, kg·s^{-1}·m^{-1}
μ_t—turbulent viscosity, kg·s^{-1}·m^{-1}
υ—kinematic viscosity, m^2·s^{-1}
k'—turbulence kinetic energy, m^2·s^{-2}
ε—turbulent dissipation rate, m^2·s^{-3}
ϕ—viscous dissipation term, m^2·s^{-3}

Subscripts

m—mean
$mojet$—mean jet outlet
∞—fluid
s—surface
sm—surface mean

REFERENCES

1. Dewan, A., Dutta, R., and Srinivasan, B., Recent Trends in Computation of Turbulent Jet Impingement Heat Transfer, *Heat Transfer Engin.*, 2012, vol. 33, pp. 447–460.
2. Amano, R.S. and Sunden, B., *Impingement Jet Cooling in Gas Turbines*, WIT Press, 2014.
3. Chauhana, R., Singhb, T., Thakurc, N.S., Kumara, N., Kumara, R., and Kumard, A., Heat Transfer Augmentation in Solar Thermal Collectors Using Impingement Air Jets: A Comprehensive Review, *Renewable Sust. Energy Rev.*, 2018, vol. 82, pp. 3179–3190.
4. Narumanchi, S.V.J., Amon, C.H., and Murthy, J.Y., Influence of Pulsating Submerged Liquid Jets on Chip-Level Thermal Phenomena, *Trans. ASME*, 2003, vol. 125, pp. 354–361.
5. Kercher, D.S., Lee, J.B., Brand, O., Allen, M.G., and Glezer, A., Microjet Cooling Devices for Thermal Management of Electronics, *IEEE Trans. Comp. Pack. Technol.*, 2003, vol. 26, pp. 359–366.
6. Freidman, S.J. and Mueller, A.C., Heat Transfer to Flat Surfaces, *General Discussion on Heat Transfer*, London: Institution of Mech. Engineers, pp. 138–142, 1951.
7. Kezios, S.P., Heat Transfer in the Flow of a Cylindrical Air Jet Normal to an Infinite Plane, Ph.D.Thesis, Illinois Institute of Technology, 1956.
8. Argus, E., Rady, M.A., and Nada, S.A., A Numerical Investigation and Parametric Study of Cooling an Array of Multiple Protruding Heat Sources by a Laminar Slot Air Jet, *Int. J. Heat Mass Transfer*, 2006, vol. 28, pp. 787–805.
9. Lee, H.G., Yoon, H.S., and Ha, M.Y., A Numerical Investigation on the Fluid Flow and Heat Transfer in the Confined Impinging Slot Jet in the Low Reynolds Number Region for Different Channel Heights, *Int. J. Heat Mass Transfer*, 2008, vol. 51, pp. 4055–4068.
10. Yang, Y.T., Wei, T.C., and Wang, Y.H., Numerical Study of Turbulent Slot Jet Impingement Cooling on a Semi-Circular Concave Surface, *Int. J. Heat Mass Transfer*, 2011, vol. 54, pp. 482–489.
11. Huang, X., Yang, W., Ming, T., Shen, W., and Yu, X., Heat Transfer Enhancement on a Microchannel Heat Sink with Impinging Jets and Dimples, *Int. J. Heat Mass Transfer*, 2017, vol. 112, pp. 113–124.
12. Olsson, E.E.M., Ahrne', L.M., and Tragardh, A.C., Flow and Heat Transfer from Multiple Slot Air Jets Impinging on Circular Cylinders, *J. Food Engin.*, 2005, vol. 67, pp. 273–280.
13. Mushatat, K.S., Analysis of the Turbulent Flow and Heat Transfer of the Impingement Cooling in a Channel with Cross Flow, *Engin. Sci.*, 2007, vol. 18, pp. 101–122.
14. Alnak, D.E., Karabulut, K., and Koca, F., Analysis of Convection Heat Transfer and Flow Properties for Air Jet Flow on Patterned Surfaces, in *Engineering and Technology*, Çam, E., Güçyetmez, M., Demirbaş, M., Lüy, M., and Barışçı, N., Eds., Ekin Printing Publishing, 2018, pp. 191–217.
15. Karabulut, K., Heat Transfer Improvement Study of Electronic Component Surfaces Using Air Jet Impingement, *J. Comput. Electronics*, 2019, vol. 18, pp. 1259–1271.
16. Afroz, F. and Sharif, M.A.R., Numerical Study of Heat Transfer from an Isothermally Heated Flat Surface due to Turbulent Twin Oblique Confined Slot-Jet Impingement, *Int. J. Thermal Sci.*, 2013, vol. 74, pp. 1–13.
17. Leena, R., Syamkumar, G., and Prakash, M.J., Experimental and Numerical Analyses of Multiple Jets Impingement Cooling for High-Power Electronics, *IEEE Trans. Comp. Pack. Manufact. Technol.*, 2018, vol. 8, pp. 210–215.
18. *FLUENT User's Guide*, Lebanon, Netherland: Fluent Inc., 2003.
19. Kilic, M., Calisir, T., and Baskaya, S., Experimental and Numerical Study of Heat Transfer from a Heated Flat Plate in a Rectangular Channel with an Impinging Air Jet, *J. Brazil. Soc. Mech. Sci. Engin.*, 2017, vol. 39, pp. 329–344.